The International Journal of Biochemistry & Cell Biology 54 (2014) 36–48

Contents lists available at ScienceDirect

The International Journal of Biochemistry & Cell Biology

journal homepage: www.elsevier.com/locate/biocel

A proteomic screen with *Drosophila* Opa1-like identifies Hsc70-5/Mortalin as a regulator of mitochondrial morphology and cellular homeostasis

Shamik Banerjee[a,b,c,*], Balaji Chinthapalli[a]

[a] *Department of Biological Sciences, Tata Institute of Fundamental Research, Homi Bhabha Road, Mumbai 400005, India*
[b] *National Center for Biological Sciences, TIFR, GKVK Campus, Bellary Road, Bangalore 560065, India*
[c] *SASTRA University, Tirumalaisamudram, Thanjavur 613402, India*

ARTICLE INFO

Article history:
Received 5 October 2013
Received in revised form 5 April 2014
Accepted 14 May 2014
Available online 1 July 2014

Keywords:
Opa1-like
Marf
Mitofilin
Mortalin
ATP synthase β-subunit
Drp-1
PKA-C1
Mitochondrial morphology
Fusion
Drosophila melanogaster
Autophagy
Cell death
Lysosome

ABSTRACT

Mitochondrial morphology is regulated by conserved proteins involved in fusion and fission processes. The mammalian Optic atrophy 1 (OPA1) that functions in mitochondrial fusion is associated with Optic Atrophy and has been implicated in inner membrane cristae remodeling during cell death. Here, we show *Drosophila* Optic atrophy 1-like (Opa1-like) influences mitochondrial morphology through interaction with 'mitochondria-shaping' proteins like Mitochondrial assembly regulatory factor (Marf) and *Drosophila* Mitofilin (dMitofilin). To gain an insight into Opa1-like's network, we delineated bonafide interactors like dMitofilin, Marf, Serine protease High temperature requirement protein A2 (HTRA2), Rhomboid-7 (Rho-7) along with novel interactors such as Mortalin ortholog (Hsc70-5) from *Drosophila* mitochondrial extract. Interestingly, RNAi mediated down-regulation of *hsc70-5* in *Drosophila* wing imaginal disc's peripodial cells resulted in fragmented mitochondria with reduced membrane potential leading to proteolysis of Opa1-like. Increased ecdysone activity induced dysfunctional fragmented mitochondria for clearance through lysosomes, an effect enhanced in *hsc70-5* RNAi leading to increased cell death. Over-expression of *Opa1-like* rescues mitochondrial morphology and cell death in prepupal tissues expressing *hsc70-5* RNAi. Taken together, we have identified a novel interaction between Hsc70-5/Mortalin and Opa1-like that influences cellular homeostasis through mitochondrial fusion.

1. Introduction

With two distinct structural and functional membranes, mitochondria reorganize into various shapes thereby influencing cellular metabolism, energy production and calcium homeostasis within a cell (Rizzuto et al., 2000; Danial and Korsmeyer, 2004). Mitofusins (Mfn-1 and -2) in the outer mitochondrial membrane (OMM) tether opposing mitochondria, following which mitochondrial targeted Phospholipase D (MitoPLD) functions *in trans* on the Cardiolipin present on opposing membranes to generate Phosphatidic acid (PA) leading to fusion of two opposing mitochondria (Choi et al., 2006). On the other hand, Dynamin related protein-1(Drp-1), a large cytosolic GTPase, is essential for scission of mitochondria (Imoto et al., 1998; Karbowski et al., 2002). The diverse inner mitochondrial membrane (IMM) compartmentalizes into boundary membrane and cristae separated by a junction, which harbor a growing family of 'mitochondria-shaping' proteins. Optic Atrophy 1 (OPA1), the only Dynamin family protein identified in the IMM is, however, involved in fusion (Olichon et al., 2002). OPA1 not only promotes mitochondrial fusion by cooperating with Mfn-1 (Cipolat et al., 2004), but also inhibits apoptosis through maintenance of cristae junctions by forming oligomers [preventing mobilization of Cytochrome c (Cyt c) on induction of apoptosis] which are

Abbreviations: OPA1, Optic atrophy 1; Cyt c, Cytochrome c; dMitofilin, *Drosophila* Mitofilin; IR, UAS driven inverted repeats, Serine protease; HTRA2, high temperature requirement protein A2; Marf, mitochondrial assembly regulatory factor; CCCP, Carbonylcyanide m-chlorophenylhydrazone; TMRM, Tetramethyl rhodamine methyl ester; IMM, Inner mitochondrial membrane; OMM, Outer mitochondrial membrane; AMP, Adult Midgut Progenitors of *Drosophila*; TORC, Target of Rapamycin Complex; cAMP-dependent PKA, cyclic Adenosine Mono Phosphate dependent protein kinase A; NMDA, N-methyl-D-aspartate.

* Corresponding author at: Department of Biological Sciences, Tata Institute of Fundamental Research, Homi Bhabha Road, Mumbai 400005, India.
E-mail addresses: shamik.sbanerjee@gmail.com, shamik.ncbs.tifr@gmail.com (S. Banerjee).

http://dx.doi.org/10.1016/j.biocel.2014.05.041
1357-2725/

regulated by the function of Rhomboid protease (Frezza et al., 2006). The cristae harbor complexes of respiratory chain components: sites for oxidative phosphorylation. Apart from holding Cyt c within cristae, Mgm1p (OPA1 ortholog in *Saccharomyces cerevisiae*) functions in regulating ATP synthase assembly and cristae morphology (Amutha et al., 2004). The other newly identified IMM protein responsible for cristae junction maintenance is Mitofilin (Rabl et al., 2009).

Mostly OPA1's (and its orthologs) function has been studied in the context of neuronal cell/tissue physiology. For instance, extracellular glutamate levels acting on NMDA receptors yields enhanced calcium influx resulting in death of neurons, which is rescued by OPA1 gain-of-function (Jahani-Asl et al., 2011). Modulation of OPA1 and abnormal cristae structures linked to mitochondrial dysfunction are attributes of neuronal cells in mouse models for Parkinson's and Huntington's disease (Kieper et al., 2010). However, few studies implicate OPA1's role in determining mitochondrial morphogenesis in non-neuronal tissues (McQuibban et al., 2006; Dorn et al., 2011). Heterozygous mutations of *Drosophila* OPA1 (Opa1-like) in whole fly showed decreased life span due to increased Reactive Oxygen Species (ROS) production emphasizing the possible roles for OPA1 in non-neuronal tissues (Tang et al., 2009). Here, we show that Opa1-like maintains mitochondrial morphology in *Drosophila* through regulated interaction with Marf (Mitofusin ortholog in *Drosophila*) and dMitofilin (Mitofilin ortholog in *Drosophila*). We show *in vitro* that loss of membrane potential induces proteolytic cleavage of Opa1-like. Using mass spectrometry, we identify some known and novel interactors of Opa1-like from *Drosophila* larval mitochondrial extracts. *Drosophila* Mortalin ortholog Hsc70-5 (Heat shock 70 kDa protein cognate 5) identified in the proteomic screen, on depletion, yields fragmented, dysfunctional mitochondria which are susceptible to degradation. Treatment of peripodial cells depleted of *hsc70-5*, with ecdysone agonist triggers lysosome-mediated cell death. The severe phenotype of both increased lysosomal activity and cell death caused by depletion of *hsc70-5* is reversed by changing the mitochondrial morphology via manipulation of mitochondrial remodeling proteins.

2. Materials and methods

2.1. Drosophila stocks

Drosophila melanogaster stocks were grown in cornmeal agar bottles and vials in 12/12 h light/dark cycles at 25 °C or as otherwise indicated. UAS-OPA1 (C-terminally Flag tagged) was kindly gifted by Dr. Jongkyeong Chung (KIASK, Korea). *marfDf* [Df(1)dx81, BL#5281, (Park et al., 2009)], *opa1*^{EP} [(P{EPgy2}Opa1-like^{Ey09863}/Cyo), BL#20054, (Park et al., 2009)], *dmitofilinDf* [Df(3R)hh^{E23}/Tm3,Sb], esg-GAL4 (DGRC#104863), UAS-mito-GFP stocks (both on 2nd and 3rd chromosome) and TubGAL4/Tm6B, Tb were obtained from NCBS fly stock facility. UAS-dsRNA constructs were co-expressed together with UAS*Dicer2* to enhance RNAi activity in prepupal tissues (Dietzl et al., 2007).

UAS-IR lines: Opa1-like (KK106290); dMitofilin (KK106757); Hsc70-5 (KK106236); Drp-1 (GD44156); Rho-7 (GD45847); pka-C1 (KK108966). GD and KK lines are from the VDRC (Vienna) collection.

2.2. Imaging

2.2.1. Cells

Hemocytes were stained with primary antibodies, anti-OPA1 (abcam, 1:200) and anti-Mitofilin (abcam, 1:200) and imaged using a confocal microscope [63× objective, 1.4NA on LSM510 Meta; Carl Zeiss (Goyal et al., 2007)].

2.2.2. Drosophila wing imaginal disc

Late 3rd instar larval wing imaginal discs were dissected in 1× PBS (10 mM NaH_2PO_4/Na_2HPO_4, 175 mM NaCl, pH7.4) supplemented with 1.5 mg/ml BSA and 1:100 dilution of Protease inhibitor cocktail (Set III; Merck), further treated with or without 1 mM 20-hydroxyecdysone (Sigma) for 2 h (22 °C). The wing imaginal discs were stained with 100 μM LysoTracker Red DND-99 (Molecular Probes) after 3 min of fixation in 3% formaldehyde [(Polysciences, Inc.); Rusten et al., 2004] along with 16.2 μM Hoechst33342 [Molecular Probes] in 1× PBS for 10 min, rinsed in 1× PBS, mounted in a drop of 1× PBS, and immediately imaged. Images were obtained using 63× objective, 1.4NA on confocal microscope, LSM510.

2.2.3. Cell Death and Quantification

Late 3rd instar larval wing imaginal discs were treated with or without 20-hydroxyecdysone (4 h) in Schneider's insect medium (Invitrogen) and later stained with 16.2 μM Hoechst33342 in 1× PBS followed by 3 μg/ml acridine orange [AO; (5 min)] and manually counted from optical sections derived from confocal microscope (LSM710) images obtained using 20× objective/0.5NA.

The numbers of fixed anti-cleaved active Caspase-3 (1:100, Sigma) positive AMPs of different genotypes of 3rd instar larval guts were manually counted from optical sections. The mean score of the wild-type control group was set as 100%, and the values of the other genotype groups were expressed as percentage compared to wild-type. Images were obtained using 63× objective/1.4NA on confocal microscope, LSM510.

2.3. Mitochondrial morphology and membrane potential assay

Collagen-GAL4 (CgGAL4; Hemocytes) and Tubulin-GAL4 (TubGAL4; Wing Imaginal Disc) were used to express UAS-Mito-GFP (mitochondrial structures inheriting matrix-targeted GFP) for mitochondrial morphology characterization.

Hemocytes were incubated with 10 nM TMRM diluted in SCM (Schneider's insect medium supplemented with 10% non-heat-inactivated fetal bovine serum and 1 μg/ml of bovine pancreatic insulin) with or without 5 μM Oligomycin (15 min) and were exposed to 543 nm light on wide-field microscope [100×, 1.4 NA objective on Nikon TE2000-U inverted microscope equipped with Andor 512B EM-CCD camera (Andor Technology) controlled by Metamorph software (Molecular Devices Corporation)]. Time-lapse images were acquired every 2 s until all mitochondrial structures released TMRM.

Isolated wing imaginal disc were incubated with 25 nM TMRM diluted in 1× PBS (supplemented with 1.5 mg/ml BSA) for over 20 min at room temperature, allowing the dye to equilibrate in cytoplasm and mitochondria (Noguchi et al., 2011, Fig. S2C). Optical sections of mitochondria in peripodial cells ($n \sim 5$–8) were collected using 40×/1.3NA objective (Zoom = 6) LSM710 Meta with 568 nm laser yielding a RAW image. Thereafter, background correction revealed a mitochondrial staining pattern [background corrected image (BCI)]. BCI was converted into a binary (BIN) image by optimizing contrast [Linear contrast (LC) to reassign the gray values from 0 to 255] in BCI, followed by median filtering and thresholding (Th). Then, the BIN image was combined with the BCI to create a masked image (MI) using a Boolean AND operation which increases the number of black pixels and removes low-intensity TMRM pixels from the BCI. Normalized mean fluorescence intensity of TMRM within MI region for mitochondria were measured and compared among genotypes using Metamorph software. Control (Ctrl) wing imaginal discs were incubated with 2 μM CCCP (Sigma) for 20 min to quench mitochondrial membrane potential and subsequently mean fluorescence intensity of TMRM was measured as described above.

Using Metamorph, mitochondrial structures were outlined and quantified and compiled using Photoshop.

2.4. Biochemical analysis

2.4.1. Purification of mitochondria and Western blotting

Crude and enriched mitochondrial fractionation from 3rd instar *Drosophila* larvae was performed by differential centrifugation and discontinuous sucrose density gradient centrifugation [(Meisinger et al., 2000; Iyengar et al., 2002), Fig. S1C]. 50 μg proteins from purified mitochondrial membrane fraction were immuno-blotted along with crude mitochondria and Heavy membrane (Hm). Blots were probed with antibodies – anti-Lamin (abcam;1:500), -DE-Cadherin (DSHB; 1:500), -Syx16 (abcam; 1:200), -Calnexin (abcam; 1:500), -KDEL (Merck; 1:500), -OPA1 (abcam; 1:200), -Mitofilin (abcam; 1:200), -Mfn-2 (abcam; 1:200), -HSP60 (HSPD1, Sigma; 1:1500), -ATPB (abcam; 1:1000), -Porin (abcam; 1:500) and -Cyt c (Invitrogen; 1:500) – against proteins of Mitochondria and other membranes as indicated in figure legends.

To evaluate the change in levels of Opa1-like, crude mitochondria were extracted from late 3rd instar larval wing imaginal discs and probed against anti-OPA1 antibody followed by re-probing with anti-ATPB (abcam) antibody.

2.4.2. Proteolysis of Opa1-like

Pelleted mitochondrial fraction (0.5 mg/ml) was incubated 20 min at 25 °C in experimental buffer [EB: 125 mM KCl (Merck), 10 mM Tris–MOPS, (pH 7.4), 1 mM Pi (Merck), 5 mM glutamate, 2.5 mM malate, 10 μM EGTA] containing 0.1%w/v azide (Baricault et al., 2007). Pre-incubations were performed with 5 mM ATP, 0.5 mM *o*-phe, 5 μM MG132 and 10 μM CCCP, for 20 min at 25 °C. After incubations, mitochondrial fractions were pelleted at 16,200 × *g* for 15 min at 4 °C. The pellet was analyzed and equivalent volumes containing 50 μg of mitochondrial proteins were separated by SDS-PAGE followed by immuno-blotting with anti-OPA1 antibody. Unless otherwise stated, all the reagents used to treat mitochondrial fractions were from Sigma.

2.4.3. Co-immuno-precipitation

Enriched mitochondrial membranes (500 μg of protein) either treated with or without 5 μM Oligomycin were solubilized (1 h, 2 °C) in lysis buffer (0.1 M NaCl, 15 mM HEPES, 0.5% Triton X-100) containing 1 mM Protease inhibitor cocktail (Set III; Merck) and pelleted (3000 × *g*; 3 min). The supernatant was incubated with 50 μg of anti-OPA1 antibody (2 h) at 4 °C and further with Protein-A beads (Pierce) for 2 h at 4 °C. Beads coupled to IgG were pelleted, washed with 1× PBS, supplemented with or without 0.2 mM DTT to release the protein precipitates (3times) from beads. The DTT-induced eluent was incubated with water:methanol:chloroform (4:4:1, v/v), the interface was further precipitated with methanol and air-dried. The air-dried sample was immuno-blotted against anti-OPA1, -Mfn-2, -ATPB and -Mitofilin antibodies.

For DTT free immuno-precipitation, beads once washed with 1× PBS (free of DTT) were suspended in Laemmli sample buffer (free of DTT) and separated by SDS-PAGE for protein identification.

2.5. Protein identification

2.5.1. In-gel digestion

The excised bands (precipitates without DTT; Fig. 2B) from the SDS-PAGE gel after colloidal Coomassie staining were sliced into smaller gel plugs. The gel plugs were destained with 50 mM ammonium bicarbonate (NH_4HCO_3, Sigma) buffer in 50% acetonitrile (Merck) and were subjected to a reduction using 10 mM dithiothreitol (DTT, Sigma) in 50 mM NH_4HCO_3 with 10% acetonitrile buffer (1 h at 56 °C). Alkylation was performed with 55 mM Iodoacetamide (Sigma) in 50 mM NH_4HCO_3 (45 min at room temperature in the dark) followed by in-gel digestion with 20 μl of trypsin (20 ng/μl, Sigma) in 50 mM NH_4HCO_3 (overnight at 37 °C). The peptides were extracted in 55% acetonitrile and 5% formic acid. Samples were vacuum-dried and reconstituted in 0.1% formic acid in water (Milli Q water, Millipore).

2.5.2. Mass spectrometry and database searching

All digested protein samples were analyzed on an Agilent 1200 SL Rapid Resolution LC coupled to an ESI Agilent 6520 Q-TOF. Briefly, samples were desalted with ZipTip C18 Columns (Pierce) before injecting into the Mass Spectrometer. The samples (2 μl) were loaded onto an Agilent nano HPLC C18 CHIP (G4240-62002). The peptides were eluted from analytical column by linear gradient of 97% Solvent A (0.1% formic acid in H_2O) to 3% Solvent A and Solvent B (90% acetonitrile with 0.1% formic acid). The data was acquired in a data-dependent mode with 4 MS spectrum followed by 3 MS/MS spectra in positive mode. *m*/*z* range used was 50–1700. MS/MS experiment was performed using collision induced dissociation (CID) in quadrupole and fragmented ions were detected in the time of flight (TOF). Data analysis was performed using Agilent Masshunter analysis software. For identification of proteins, the .mgf file was searched against *Drosophila melanogaster* database from SwissProt using an in-house Mascot server (version 2.3.02) with the peptide mass tolerance set as 10 ppm and MS/MS mass tolerance 0.6 Da; cysteine carbamidomethylation as fixed modification.

2.6. RT-PCR

RNA was ethanol precipitated from TRIZOL, extracted from 50 late 3rd instar larval wing imaginal discs. The primers used in the PCR are detailed (Fig. S3C). Equal volumes of the PCR product were run on the same gel, the DNA quantified using Metamorph software and represented relative to the amount of rp49 RNA.

2.7. Genotypes

Hemocyte culture-

+/+; Cg GAL4/+; UAS mito-GFP/+ (Ctrl)
+/+; Cg GAL4/*UAS-opa1-like* IR; UAS mito-GFP/+ (*opa1-like*↓)
+/+; Cg GAL4/*UAS-dmitofilin* IR; UAS mito-GFP/+ (*dmitofilin*↓)
+/+; Cg GAL4/+; UAS mito-GFP/UAS *OPA1-FLAG* (*opa1-like*↑)

Larval Wing Imaginal Disc-

UAS-Dicer2/+; UAS mito-GFP/+; Tub GAL4/+ (Ctrl)
UAS-Dicer2/+; UAS mito-GFP/UAS-*opa1-like* IR; Tub GAL4/+ (*opa1-like*↓)
UAS-Dicer2/+; UAS mito-GFP/UAS-*dmitofilin* IR; Tub GAL4/+ (*dmitofilin*↓)
UAS-Dicer2/+; UAS mito-GFP/+; Tub GAL4/UAS *OPA1-FLAG* (*opa1-like*↑)
UAS-Dicer2/+; UAS mito-GFP/UAS-*hsc70-5* IR; Tub GAL4/+ (*hsc70-5*↓)
UAS-Dicer2/+; UAS mito-GFP/UAS-*hsc70-5* IR; Tub GAL4/UAS-*OPA1-FLAG* (*hsc70-5*↓; *opa1-like*↑)
UAS-Dicer2/+; UAS mito-GFP/UAS-*hsc70-5* IR; Tub GAL4/UAS-*drp-1* IR (*hsc70-5*↓; *drp-1*↓)
UAS-Dicer2/+; UAS-*pKa-C1* IR/+; Tub GAL4/UAS mito-GFP (*pka*↓)
UAS-Dicer2/+; UAS-*pKa-C1* IR/UAS-*hsc70-5* IR; Tub GAL4/UAS mito-GFP (*hsc70-5*↓, *pka*↓)

Larval Gut-

UAS-Dicer2/+; esg GAL4/+; UAS mito-GFP/+ (Ctrl)
UAS-Dicer2/+; esg GAL4/UAS-*opa1-like* IR; UAS mito-GFP/+ (*opa1-like*↓)
UAS-Dicer2/+; esg GAL4/UAS-*hsc70-5* IR; UAS mito-GFP/+ (*hsc70-5*↓)

UAS-Dicer2/+; esg GAL4/UAS-*hsc70-5* IR; UAS mito-GFP/*UAS-OPA1-FLAG* (*hsc70-5*↓; *opa1-like*↑)

UAS-Dicer2/+; esg GAL4/UAS-*hsc70-5* IR; UAS mito-GFP/UAS-*drp-1* IR (*hsc70-5*↓; *drp-1*↓)

UAS-Dicer2/*dor*^{4}; esg GAL4/UAS-*hsc70-5* IR; UAS mito-GFP/+ (*dor*^{4}; *hsc70-5*↓)

2.8. Statistics

Data was compared using either Student's *t*-test or one-way ANOVA with Tukey multiple comparison test. Differences were considered to be significant if $p < 0.05$. Graphs represented were made using Excel and Matlab software.

3. Results and discussion

3.1. Characterization of Drosophila OPA1 and Mitofilin in influencing mitochondrial morphology

The components involved in regulating mitochondrial morphology are conserved across species, but very little is known about their interplay in *Drosophila* mitochondria. Homology studies based on Mgm1 (yeast) and hOPA1 (human) designated CG8479 (Accession No. A1Z9N0) as fly OPA1 or Opa1-like. Opa1-like participates in nebenkern formation and its down-regulation results in mitochondrial fragmentation in *Drosophila* S2 cell line (McQuibban et al., 2006). The roles of Marf [(CG3869), 66% similar to hMfn2 (human); (Accession No. Q7YU24) shown to participate in mitochondrial morphogenesis in *Drosophila* tissues (Deng et al., 2008)] in OMM, and of *Drosophila* Mitofilin [dMitofilin (CG6455); Accession No. P91928, identified in a proteomics study (Alonso et al., 2005)] and Opa1-like in IMM, in deciding mitochondrial morphology is unclear. First, we used *Drosophila* larval hemocytes [Fig. S1A (i-ii) and S1B] to study changes in mitochondrial morphology since mitochondrial fission and fusion in *Drosophila* (Goyal et al., 2007; Ziviani et al., 2010) maintain similar organelle morphologies as those observed in yeast (Nunnari et al., 1997) and mammalian cells (Bereiter-Hahn and Voth, 1994). Down-regulation of both *opa1-like* and *dmitofilin* resulted in fragmented mitochondria (in ~80% of hemocytes, CSA<2.5 μm^2); whereas over-expression of *Opa1-FLAG* resulted in almost equal proportion of cells with extremely tubular (CSA>5.0 μm^2) and clumped (Santel and Fuller, 2001) mitochondria as observed with Tetramethyl rhodamine methyl ester [TMRM; Fig. 1A and Fig. S1A] staining.

Then, we took a targeted approach to characterize Opa1-like and its known binding partners – fly orthologs of Mitofusins and Mitofilin – using commercially available antibodies [Figs. 1B; Fig. S1E(i, ii and iii)] by Western blotting on enriched (purified) mitochondria compared to crude [Mt and Mt^{c} (2-3 fold enrichment) respectively] and also by immuno-fluorescence confocal microscopy in hemocytes of *Drosophila melanogaster* [Figs. 1C(i-vi) and Fig. S1F(i-ii)]. Sub-cellular analysis indicated that the enriched mitochondrial fraction (Mt) was positive for Cyt c, Hsp60, Porin, b-subunit of ATP synthase (ATPB), Opa1-like and Mitofilin, but was negative for dLamin, DE-Cadherin, dSyx16 and dKDEL (mainly marks Grp78), thus eliminating possibility of contamination from other cellular components in Mt (Figs. 1B, Fig. S1D). On SDS-PAGE from Mt, specific bands of Opa1-like migrate as ~90 kDa [PA- Isoform A; Fig. 1B, Fig. S1E(i)] and ~110 kDa [PB-Isoform B; Figs. 1B and S1E(i); (Rahman and Kylsten, 2011)]; whereas Marf migrates as ~90 kDa [Figs. 1B and S1E(iii) Rana et al., 2013] and dMitofilin migrates as ~80 kDa band [Figs. 1B and S1E(ii)]. Opa1-like, Marf and dMitofilin specificities were confirmed by Western blotting (Fig. S1E) and RT-PCR (Figs. S3A and S3B) from both depleted background and deficiency/deletion mutants [*marf Df*- {Df(1)dx81) - cytological break point 5C1-6C12} and *dmitofilin Df*- {Df(3R)hh^{E23}- cytological break point 94A-94D1} Fig. S1E(ii,iii)]. However, immuno-blotting results indicate ~150 (inconsistent), 55 and 70 kDa bands being non-specific with the commercial antibodies against OPA1, Mfn-2 and Mitofilin respectively [Fig. S1E(i,ii,iii)]. Quantitative fluorescence imaging with anti-OPA1 and -Mitofilin antibodies showed significant changes in both RNAi (IR; expression of UAS-hairpin transgene/inverted repeats) and over-expression backgrounds (Figs. 1C and S1G), consistent with Western blotting analysis, which validates the use of these antibodies in *Drosophila*.

OPA1 regulates mitochondrial fusion through cooperative activity of long and short isoforms (Song et al., 2007). Disruption of mitochondrial membrane potential or activation of apoptosis induces OPA1 processing (Duvezin-Caubet et al., 2006; Baricault et al., 2007) by proteases in the IMM (McQuibban et al., 2006; Tatsuta and Langer, 2008). Isolated enriched mitochondria from 3rd instar larvae, on treatment with the protonophore [Carbonylcyanide m-chlorophenylhydrazone (CCCP)] which induces loss of mitochondrial membrane potential, resulted in different sizes of Opa1-like bands ranging from ~80 to 50 kDa [Fig. 1D] -indicating Opa1-like processing in *Drosophila* tissues. The maximal conversion of both the isoforms into proteolytic products was delayed or inhibited by the combined use of specific protease inhibitors like membrane-permeable metalloprotease inhibitor [*o*-phenanthroline (*o*-phe)] and proteasome inhibitor (MG132), or by down-regulation of *rho-7* [Rhomboid-7; *Drosophila* homologue of PARL; Rahman and Kylsten, 2011; Ehses et al., 2009 and Figs. 1D and S1E(iv)].

Both in yeast and mammals, Fzo1p (Mfn-1,-2) and Mgm1p (OPA1) were shown to interact reciprocally (Sesaki et al., 2003; Wong et al., 2003; Guillery et al., 2008) suggesting a physical association between both the outer and inner membranes post fission. However, a recent report on mammalian OPA1 interaction with Mitofilin and ChChd3 in the IMM alone indicates the proteins' role in cristae junction maintenance (Darshi et al., 2011). Specific protein complexes involved in interaction between *Drosophila* mitochondrial structures or compartments have not yet been reported.

3.2. Proteomic screen identifies Hsc70-5/mortalin, Marf, Mitofilin, ATPB as Opa1-like interactors from mitochondrial extracts

While searching for proteins that function through an Opa1-like-mediated mitochondrial role in a cellular context, we carried out immuno-precipitation of endogenous Opa1-like from enriched mitochondria of 3rd instar *Drosophila* larvae using anti-OPA1 polyclonal antibody. The immuno-precipitated fraction was first resolved using SDS-PAGE (visualized by Coomassie blue G-250; Fig. 2B) followed by tryptic digest of excised gel pieces which were directly subjected to LC-coupled ESI Q-TOF mass spectrometry. A complex protein profile [~93% mitochondrial proteins (~39% IMM resident proteins); Fig. 2C], was obtained on analysis of the peptides (Supplementary Table 1), consistent with the ability of Opa1-like to interact with a variety of partners that included ~90 and 106 kDa bands, recognized to be Opa1-like isoforms, which act as positive control (Fig. 2B and D). In particular, the bands ~52, 90, and 120 kDa yield peptides of dATP synthase β-subunit (ATPB), Marf (PC), and a probable complex of dMitofilin with dTom40 (von der Malsburg et al., 2011; Fig. 2B; Table.1) respectively. The ability of Opa1-like and dMitofilin to interact with each other was validated by immuno-precipitation followed by Western blot analysis (Fig. 2D and E, Darshi et al., 2011).

Surprisingly, the interaction (revealed by targeted approach) of *Drosophila* Opa1-like with Marf, dMitofilin and dATP synthase b-subunit (ATPB), which also validates the proteomic screen, turned

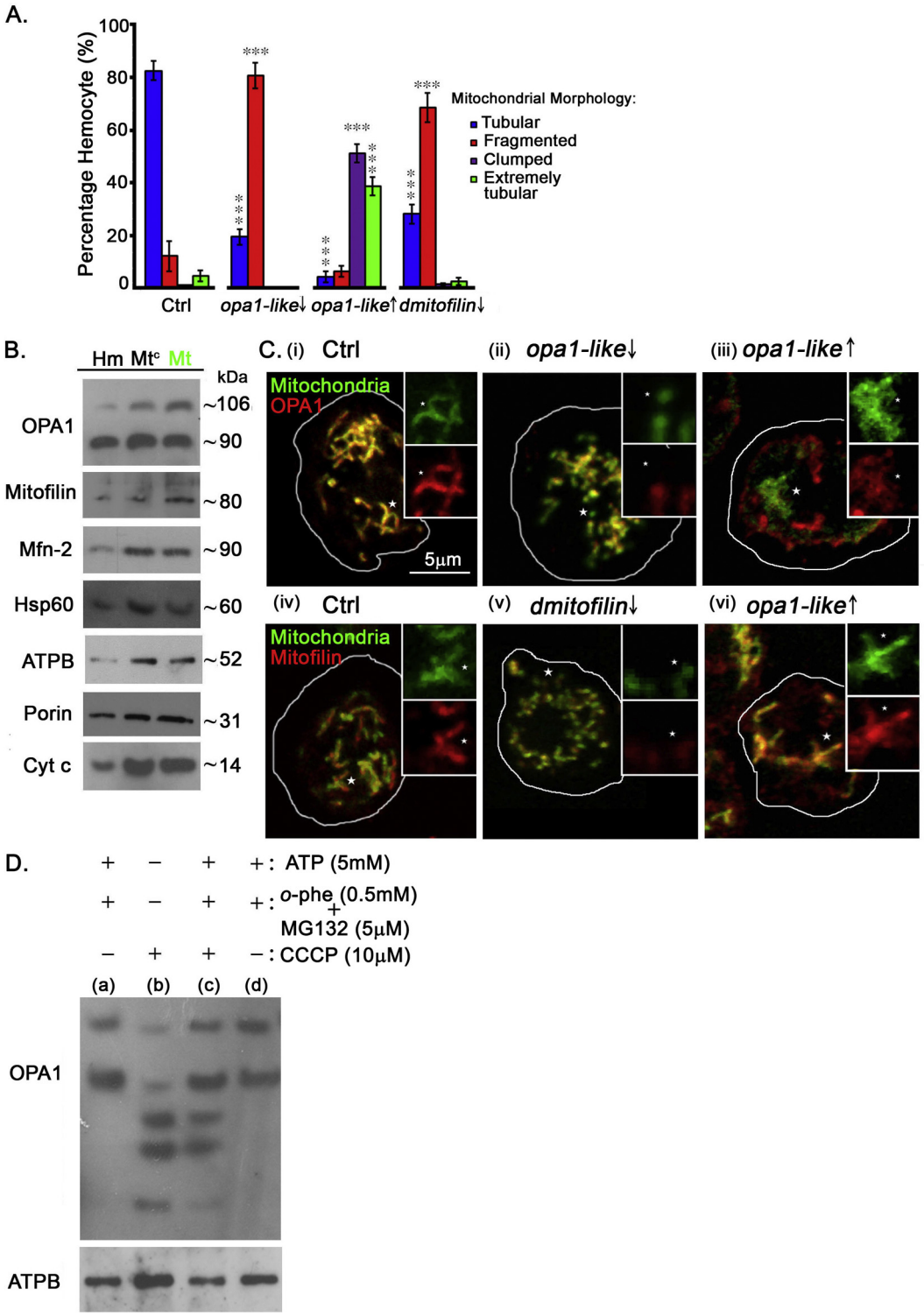

Fig. 1. *Drosophila* Opa1-like influences mitochondrial morphology. (A) Mitochondria visualized as Mito-GFP or TMRM positive compartments in hemocytes are categorized based on mitochondrial morphology as tubular, fragmented, extremely tubular or clumped. Histograms show the number of hemocytes (as percentage; Mean ± SEM; $N = 3$, $n \geq 30$) derived from Control (Ctrl), *opa1-like*↓, *opa1-like*↑ and *dmitofilin*↓ larvae (29 °C) categorized as tubular (blue), fragmented (red), clumped (purple) and extremely tubular (green). *P* value $^{**}<0.05$, $^{***}<0.005$. (B) Evaluation of enriched mitochondria (Mt) from Crude mitochondrial pellet (Mt^c) and heavy membrane (Hm) fraction using specific antibodies against various mitochondrial proteins. The antibodies used to detect endogenous Porin and Mfn-2 (label OMM), OPA1, Mitofilin and ATPB (label IMM), Cyt-c (labels IMS) and Hsp60 (labels mitochondria matrix). Note that there is ~2–3 fold enrichment of mitochondrial proteins, in Mt compared to Hm and no detectable contamination of indicated intracellular membranes (Fig. S1D). (C) Merged confocal images of Mito-GFP (green) expressing hemocytes derived from Ctrl, *opa1-like*↓, *opa1-like*↑ and *dmitofilin*↓ larvae (29 °C) stained with anti-OPA1 (i, ii and iii) or -Mitofilin (iv, v and iv) antibodies (red) colocalize with mitochondria. Insets are a magnified view of the indicated area (asterisk). Scale 5 μm, 1.5 μm (inset). D) Stability of Opa1-like in the presence of different protease inhibitors reveals proteolytic products of Opa1-like. Western blot performed on purified mitochondrial fractions (50 μg) pre-treated (+) with or (−) without ATP, *o*-phenanthroline (*o-phe*) and MG132; subsequent incubation in experimental buffer (a), with m-chloro-carbonylcyanide-phenylhydrazine [(CCCP); (b) and (c)]. Purified mitochondria derived from UAS-*rho-7* IR (d) acts as negative control.

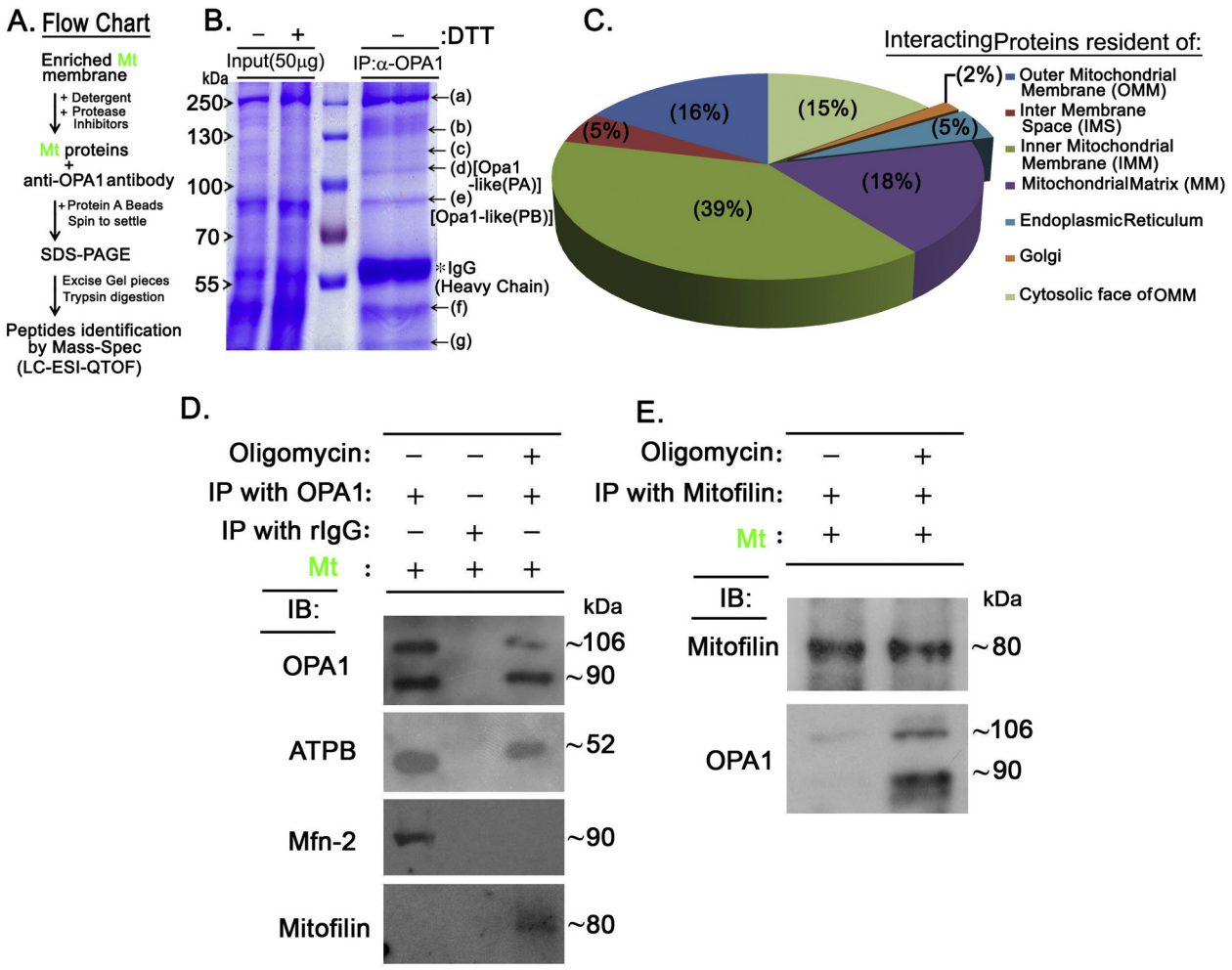

Fig. 2. Opa1-like's interacting profile. (A) Flow chart shows experimental procedure to identify Opa1-like interacting proteins. (B) OPA1-like IP was performed from enriched mitochondrial protein derived from *Drosophila* 3rd instar larvae using polyclonal anti-OPA1 antibody and Coomassie stained for proteomics analysis. Arrows indicate excised bands for proteins identification by mass spectrometry. Note that the ~106 kDa (d) and ~90 kDa (e) bands in IP lane are identified as Opa1-like isoforms. Asterisk marks heavy chain of IgG. Arrow-head indicates the band sizes of protein ladder. (C) Pie chart indicates profiling of Opa1-like interacting proteins. (D) Purified mitochondrial pellet from *Drosophila* 3rd instar larvae immunoprecipitated (IP) using either anti-OPA1 or anti-rabbit IgG (IP control) antibodies in the presence or absence of Oligomycin and probed with anti-OPA1, anti-ATPB, anti-Mfn-2 and anti-Mitofilin antibodies. (E) Purified mitochondrial pellet immunoprecipitated using anti-Mitofilin antibody in the presence or absence of Oligomycin and probed with anti-OPA1 and anti-Mitofilin antibodies. Functional state of mitochondria determines paired interactions between Opa1-like1 and dMitofilin, Opa1-like and Marf or Opa1-like and ATPB.

out to be an ATP dependent step (Fig.2D and E). Treatment of Mt with Oligomycin, an ATPase inhibitor, decreases interaction of Marf and ATPB with Opa1-like. Interestingly, depletion of ATP resulted in increased interaction of Opa1-like with dMitofilin. Oligomycin treatment leads to mitochondrial fragmentation in hemocytes as analyzed by TMRM (Fig.S1B). Therefore, it might imply that interactions between Opa1-like and dMitofilin or Opa1-like and Marf are part of mutually exclusive protein complexes which activate on account of their ATP dependence. Even though both Marf and Opa1-like are membrane bound GTPase proteins, apart from GTP hydrolysis, both the OMM and IMM fusion requires a proton gradient and an electrical potential at the IMM respectively (Meeusen et al., 2004). This energy dependency might lead to formation of preferential membrane contacts alternating via both interactions, thus, regulating mitochondrial morphology. Further, ATP depletion results in mitochondrial fragmentation through increased ROS leading to widening of cristae junctions and, also, depletion of both OPA1 and Mitofilin leads to Cyt c release through the cristae junctions (Frezza et al., 2006; Yang et al., 2012). Treatment with oligomycin leads to mitochondrial-network fragmentation (De Vos et al., 2005) mainly due to increase in mitochondrial and cytosolic ROS concentration (Benard et al., 2007). Thus, Opa1-like and dMitofilin interaction in an ATP depleted state probably functions to prevent opening of cristae junctions which would otherwise lead to Cyt c release and thereby activation of cell death.

Interestingly, among the interacting peptides we found 18 belonging to the fly ortholog of Mortalin – an hsp70 (Heat shock protein family) cognate subunit 5 [(CG8542); Accession No. P29845; Zhu et al., 2013]. A bioinformatics analysis for homology using HHpred (Söding et al., 2005) showed that CG8542 is orthologous to the human protein Mortalin [HSPA9B (Kaul et al., 2007)] with high probability and low E-value (Fig. S4). Even though mtHsp70 cognate 5 is an ortholog of human protein Mortalin, we have not done experiments to show that *Drosophila* mtHsp70 cognate 5 fulfils the mammalian Moratlin paradoxes (Kaul et al., 2007). Therefore, we would like to term mtHsp70 cognate 5 (CG8542) as Hsc70-5 [Flybase (http://flybase.org), Zhu et al., 2013]. Interestingly, Mitofilin and Mortalin (HSPA9) are components of the MINOS (mitochondrial inner membrane organizing system) complex, which is responsible for holding cristae membranes to the

Table 1
Some of the potential interactors of Opa1-like.

Swiss-Prot Accession No.	Protein name	Sub-cellular localization	No. of unique peptides	Peptide sequences	Sequence coverage (%)	Band on gel	Previous report on interaction
A1Z9N0 Q95U20	Opa1-like (PA) Opa1-like (PB) (CG8479)	IMM	8	AKGEILDEVVTLSQISAK ALGYYAVVTGR VLLAEELIK SDFAQAVDAGLR ARYIVR APRGSGDMK TIFVLTK QQYLILK	15.6	(d) (e)	
P91928	dMitofilin (CG6455)	IMM	18	AKPVSKPA KNRASAR KLVDHIGN LQLAGMLGK DRSDFLQA EAQERGVY PVSKPAAAAAP LATEKANYKLO KKVEAVRDKIK GDDLVAAVLESVPK TYDILNRARYHVDR GSGDDKSKKSKVEPVKATP VAIGVLKGFNDDVRKVVDKAV EQGQQGDQGYQGYQSLPPHM NVNDQIDKVKSGIETVTSTVD VDSVTSKVTGLFGGGSGDDKSKKS	44	(b) (c)	Darshi et al., 2011 (In HEK293 cells and mouse liver)
Q05825	ATP synthase subunit beta, mitochondrial (CG11154)	IMM	20	RLVLEVA EGGVISLK IGLFGGAGVG LLAPYAKGG ATTVLSRAI IGEPIDERG QEILVTGIK EGQDVLLFI LVPLEQTIK ALTGLTVAEYF IINVIGEPIDER FTQAGSEVSALLGR VALTGLTVAEYFR TVLIMELINNVAK VAQHLGENTVRTIAMDGT FLSQPFQVAEVFTGHAGK KKGSITSVQAIYVPADDLT DGTEGLVRGQKVLDTGYPI VDVQFDDNLPPILNALEVDNR	42.2	(a) (b) (f)	None
P29845	Heat shock 70 kDa protein cognate 5/Mortalin (CG8542)	Mitochondrial matrix	18	LVGDLIK GQIAGLNV LFELAYK DVLLLDVTPL AKCELSSSQQ DAGQIAGLNVLR EFKKDSGIDIR IGEVLLVGGMTRM LDVTPLSLGIETLG TRSKLESLVGDLI SKLESLVGDLIKR VYSPSQIGAFILMK ANKETADLEEVRKA LAYKKMSAERESNA SSGGLSKDEIENMIK DGERLVGMPAKRQAVT TLLANKETADLEEVRK ANKETADLEEVRKATSS	29.6	(a) (b) (f)	None
Q7YU24	Marf (CG3869)	OMM	3	AKHGSGDMK GSNLRAR LLNVLENQK	21.2	(e)	Guillery et al., 2008
A1Z8R8	Rhomboid-7 (CG8972)	IMM	3	MLSVLFK SCRQIHSNR CHANVNVPILR	5.6	(a)	None

Table 1 (*Continued*)

Swiss-Prot Accession No.	Protein name	Sub-cellular localization	No. of unique peptides	Peptide sequences	Sequence coverage (%)	Band on gel	Previous report on interaction
Q9U4L6	dtom40 (CG12157)	OMM	8	QFSARLR LPKANLVF ATLAYQIDLPKA GLDSLAAAKDAALE VVGQYLQSVTPAL HVKNNFRLGCGLMI DSLAAAKDAALENPGTVE PTEAFPVLLGDIDPAGNLNA	39	(a) (c) (g)	None
Q7YU24	Serine protease HTRA2 (CG8464)	IMS	12	FTPTIAASKMT IPIDYVKVFL IGVNSMKVTAGIS LGSPLALSNTVTAG QTDAAITFGNSGGPLV QTDAAITFGNSGGPLV LADNSKTLDIVILR LVNLDGEAIGVNSMKV ALADNSKTLDIVILRGVKQMH AAEKRKKGSAYKTGYPVKRYMG DAAITFGNSGGPLVNLDGEAIGVNSMKVTAGISFA EKGWRRLVRFFVPFSLGAAVSAAIIQREDFTP	34.1	(a) (e)	Kieper et al., 2010 (In HEK293 cells and C57/B16 mouse brain)

inner boundary membrane via crista junctions and helps in interaction of IMM with the OMM (Darshi et al., 2011). Although some Mortalin/Grp75 and VDAC1 (Schwarzer et al., 2002) on OMM and IP_3R on ER (Endoplasmic Reticulum) form a complex for calcium channeling from ER to mitochondria (Szabadkai et al., 2006), majority of the Mortalin is a part of a protein import motor in association with TIM23 in the mitochondrial matrix and functions in controlling cell proliferation and differentiation (Neupert and Brunner, 2002; Liu et al., 2005). Mortalin has been linked to age-related disorders like Parkinson's disease (PD) mainly due to reduced levels in affected brain regions of sporadic PD patients and associated impairment in mitochondrial function (Burbulla et al., 2010). Mortalin isoform HSPA9A was reported to regulate numbers of hematopoietic progenitors (non-neuronal cells; Chen et al., 2011). We, therefore, decided to probe the role of Hsc70-5 in mitochondria-linked cellular homeostasis of non-neuronal *Drosophila* cells and tissues.

3.3. Depletion of hsc70-5 influences mitochondrial morphology through Opa1-like proteolysis

Identifying the fly ortholog Mortalin, a known mitochondrial stress protein, as an Opa1-like interactor prompted us to understand its role in mitochondrial morphogenesis and its link with cellular homeostasis. Even though mitochondrial homeostasis plays a crucial role in aging and cell death, the intra-mitochondrial signaling pathways involved in cellular stress response and initiation of cell death have been poorly investigated. We used *Drosophila* prepupal tissues like wing imaginal disc and larval-gut since these tissues undergo cell death episodes during metamorphosis and the dosage of ecdysone, a component responsible for this metamorphosis, determines morphological changes in mitochondria which directly influence cellular homeostasis (Goyal et al., 2007). Mitochondria, visualized by using matrix-targeted GFP [mito-GFP; (Pilling et al., 2006; Goyal et al., 2007)], in peripodial cells of 3rd instar larval wing imaginal disc derived from UAS-*opa1-like* IR, UAS-*dmitofilin* IR and UAS-*hsc70-5* IR backgrounds were fragmented unlike the Control [Fig. 3A(i,ii)]. However, over-expressing *Opa1-FLAG* or down-regulation of *drp-1* in UAS-*hsc70-5* IR background reverses the fragmented morphology [Fig. 3A(ii)], suggesting that this fragmentation of mitochondria in UAS-*hsc70-5* IR is Drp-1-dependent. Interestingly, the loss of function of *Ssc1p* (yeast ortholog of mortalin) results in the fragmentation of the mitochondrial network (Kawai et al., 2001), suggesting similar morphological phenotypes for loss of *mortalin* function in yeast and *Drosophila* cells. The extent of depletion and up-regulation of transcripts in larval wing imaginal discs of various genotypes being used have been quantified in Fig. S3A and B. Quantification revealed a dramatic decrease in the prepupal mitochondrial cross-sectional area [CSA; Fig. 3A(i and ii)] and a significant increase in the number of mitochondria per cell in *opa1-like, dmitofilin* and *hsc70-5* RNAi.

Probing for Opa1-like levels in UAS-*dmitofilin* IR and UAS-*hsc70-5* IR larval wing imaginal discs reveals that the Opa1-like ~106 kDa band was unaffected whereas ~90 kDa band was reduced with appearance of lower sized proteolytic products [Fig. 3D(i,ii)] similar to sizes observed when Opa1-like was treated with the protonophore, CCCP [Fig. 1D]. This suggests that Opa1-like isoforms in these backgrounds undergoes proteolytic cleavage or degradation probably due to loss of membrane potential as previously demonstrated (Legros et al., 2002; Duvezin-Caubet et al., 2006; Ishihara et al., 2006; Song et al., 2007). Quantifying changes in membrane potential ($\Delta\psi_m$; O'Reilly et al., 2003) using the membrane potential-sensitive dye, TMRM, in peripodial cells of wing imaginal discs showed that normalized fluorescence of TMRM in UAS-*hsc70-5* IR is less in mitochondria [(CSA < 1.0 and >1.0 μm^2); Fig. 3B and C(i,ii)] compared to Control. *In vitro* studies replicating the cause of extensive mitochondrial network fragmentation using pharmacological uncouplers indicates that the dissipation of membrane potential ($\Delta\psi_m$) leads to proteolytic cleavage or degradation of cellular OPA1 and thereby to inhibition of fusion (Legros et al., 2002; Meeusen et al., 2004; Duvezin-Caubet et al., 2006; Ishihara et al., 2006; Song et al., 2007; Twig et al., 2008).

3.4. Rescue against lysosome mediated cell-death by mitochondrial fusion via opa1-like

Mitochondrial depolarization precedes the induction of autophagy and depolarized mitochondria undergo mitophagy (Elmore et al., 2001; Twig et al., 2008). Mito-GFP labeled mitochondria that overlap with lysosomal structures were scored for as events of mitochondrial degradation in 3rd instar larval wing imaginal discs, both in the presence or absence of inducers such as 20-hydroxyecdysone or rapamycin. Mito-GFP+ve structures (mitochondrial structures inheriting matrix-targeted GFP) colocalize with Lysotracker Red (an effective marker of both lysososomes and autolysosomes in fat body and wing imaginal disc; Scott et al.,

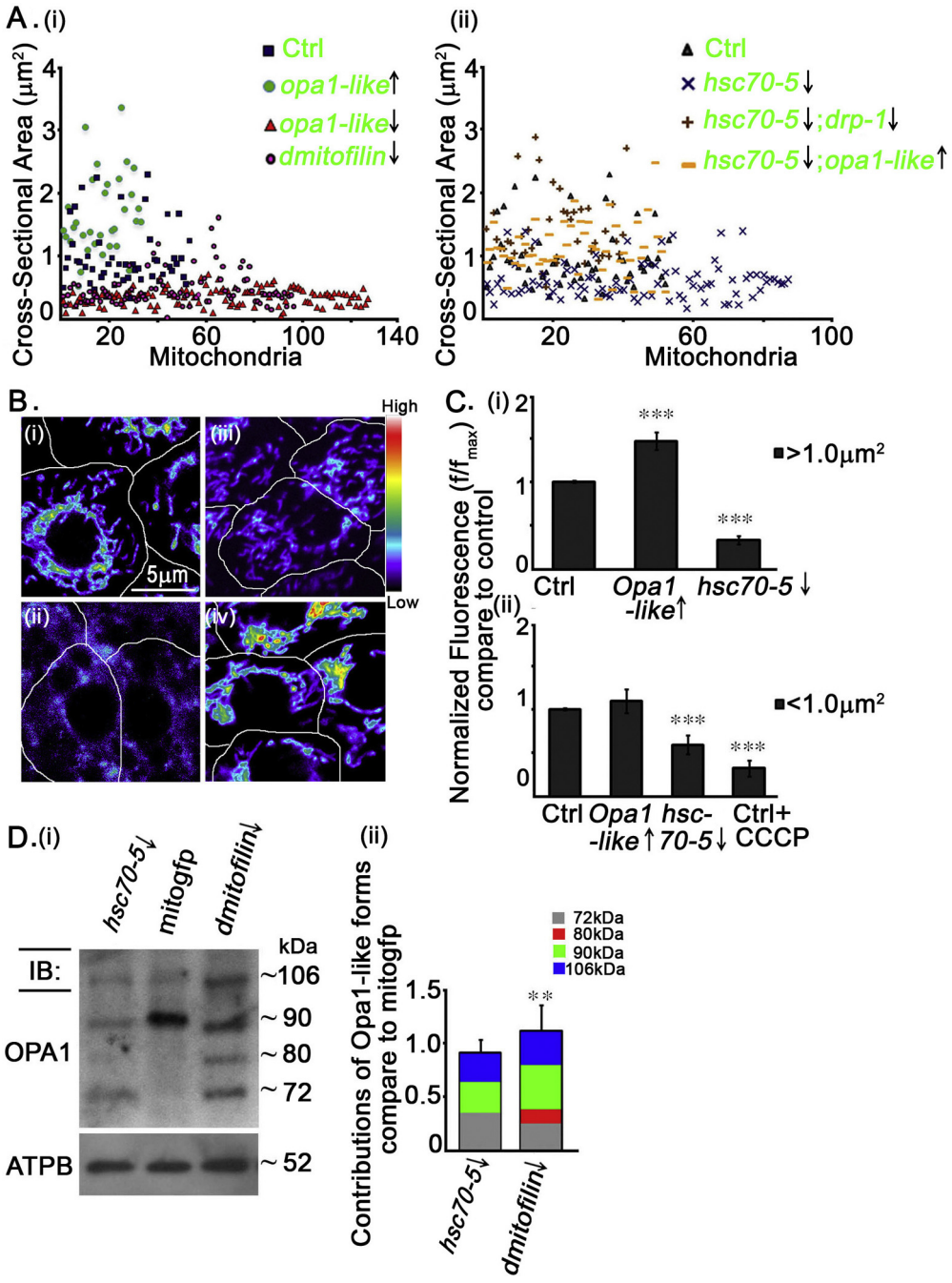

Fig. 3. Characterization of Hsc70-5/Mortalin's role in mitochondrial morphogenesis in 3rd instar wing imaginal disc of *Drosophila*. (A) Scatter plot showing mitochondrial CSA in a wing disc peripodial cells in Ctrl [(i),(ii)], *opa1-like*↓(i), *dmitofilin*↓(i), *opa1-like*↑(i), *hsc70-5*↓(ii), *hsc70-5*↓; *opa1-like*↑(ii) and *hsc70-5*↓;*drp-1*↓(ii). (B) Normalized TMRM fluorescence (f/f_{max}) in *hsc70-5*↓ (iii) and *opa1-like*↑ (iv) compared to Ctrl (i) in the mitochondria was used as a measure of mitochondrial activity (see Experimental Procedures and Fig. S2C for details). As a negative control, 2 μM of CCCP (ii) was added to suppress membrane potential of mitochondria. Scale bar 5 μm. (C) Histogram shows a quantifiable measure of mitochondrial activity in structures with CSA > 1.0 μm^2 (i) and CSA < 1.0 μm^2 ($N = 5$, $n \geq 10$ and Mean ± SEM). *P* value **<0.05, ***<0.005. [D (i)] Crude mitochondrial protein extracts (20 μg) from 3rd instar larval wing imaginal disc expressing either UAS-mito-GFP, UAS-*hsc70-5* IR or UAS-*dmitofilin* IR driven by Tub-GAL4 were subjected to western blot analysis with an anti-OPA1 antibody. The same blot was reprobed with anti-ATPB antibody as loading control. (ii) Contribution plot (Mean ± SD) of individual Opa1-like positive bands with respect to total in UAS-mito-GFP, UAS-*hsc70-5* IR and UAS-*dmitofilin* IR were compared with anti-ATPB antibody probed blot (loading control) and UAS-mito-GFP acting as normalizing factor.

2004; Rusten et al., 2004) on treatment with 20-hydroxyecdysone and rapamycin [Fig. 4A (i), (ii), (ii′) and (ix)]. The association of Mito-GFP+ve structures with Lysotracker Red structures was reversed on treatment with 3-methyladenine (3-MA) in the presence of ecdysone agonist, 20-hydroxyecdysone [Fig. 4A (ii′)]. The propensity of mitochondrial structures [CSA < 0.5 μm^2, Fig. 4A(iii,iv) and B(ii)] co-labeled with Lysotracker structures increased in UAS-*hsc70-5* IR compared to Control [Fig. 4A(i,ii) and B(ii)], with or without treatment with 20-hydroxyecdysone. Interestingly, mitochondria with CSA > 0.5 μm^2 did not overlap with Lysotracker positive structures upon rescue with over-expression of *Opa1-FLAG* in UAS-*hsc70-5* IR background [Fig. 4A(viii) and B(ii)], suggesting that tubular organelle state bypasses the degradation process (Gomes et al., 2011).

Mitochondrial fusion and autophagy are reciprocally dependent on $\Delta\psi_m$. Thus, modulating fission leads to separation of

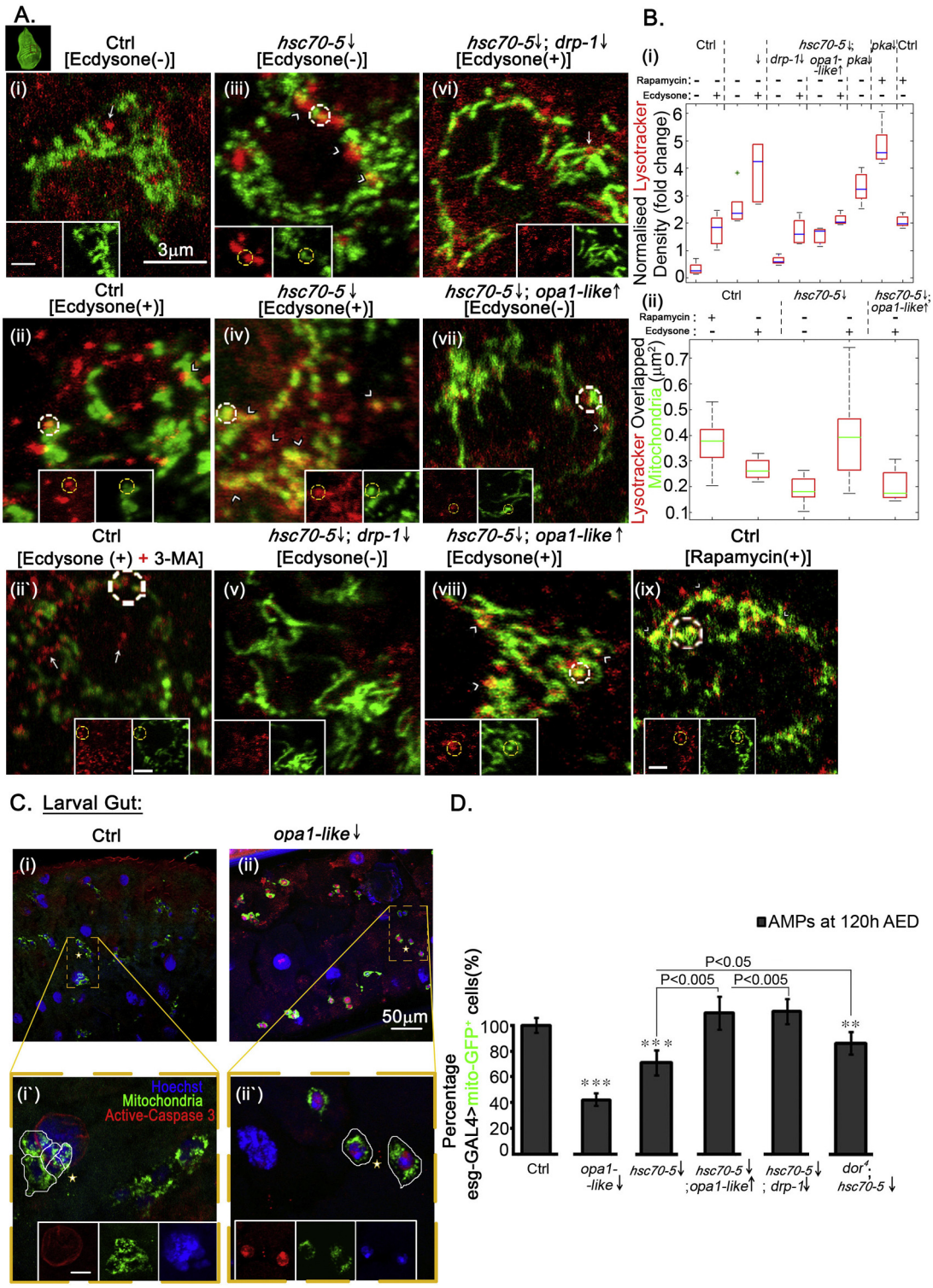

Fig. 4. Opa1-like rescues of ecdysone agonist induced lysosomal activity mediated cell death in UAS- hsc70-5 IR. (A) Single plane confocal images of wing imaginal disc mitochondria (mito-GFP) co-labeled with Lysotracker (red) in presence or absence of ecdysone in Ctrl [(i),(ii) and (ii′) {+10 mM 3-MA (3-methyladenine for 30 min after ecdysone treatment)}, (ix) {+50 μM rapamycin (for 2 h)}], *hsc70-5*↓ [(iii),(iv)], *hsc70-5*↓;*drp1*↓ [(v) (vi)], *hsc70-5*↓; *opa1-like*↑ [(vii) and (viii)]. Note that white dotted ring zoomed as insets and white arrow (i, ii′ and vi) indicates lysosomal structures. Scale bar 3 μm and 1.5 μm (inset) [Inset scale bar of (ii′) and (ix) is 3 μm]. [B (i)] Quantification of Lysotracker Red staining. The number of lysotracker-positive spots per unit area in the presence or absence of 20-hyroxyecdysone/rapamycin shown for each indicated genotype including *hsc70-5*↓, *pka*↓ and *pka*↓, normalized to the value for wild-type wing imaginal disc cells of same age were processed in parallel. (ii) Quantification of Lysotracker Red over-lapped mitochondrial (mito-GFP) structures of wing imaginal disc cells derived from genotypes indicated in (A) as white arrow head and white dotted ring, in the presence or absence of 20-hydroxyecdysone/rapamycin treatment. (C) 120hAED larval guts derived from (i, i′) Ctrl and (ii, ii′) *opa1-like*↓ containing mito-GFP+ve AMPs in clusters. Hoechst33342 (Blue) represent nuclei, and active-Caspase 3 (Red) represent dying cells marked in mito-GFP+ve single/cell-clusters shown in magnified views of the area indicated as star in a yellow box. Note that white arrow (ii) indicates mito-GFP+ve AMPs negative for anti-active-Caspase3 antibody in *opa1-like*↓. Scale bar 50 μm and 10 μm (inset) (D) Histogram shows the number of mito-GFP+ve cells harboring 120hAED larval guts (as percentage; Mean ± SEM; $N = 5$, $n \geq 30$) in various genotypes: *hsc70-5*↓, *hsc70-5*↓; *opa1-like*↑, *hsc70-5*↓; *drp1*↓, *dor*^{4}; *hsc70-5*↓ and Control. *P* value **<0.05, ***<0.005.

uncoupled mitochondria from the network (Twig et al., 2008; Gomes et al., 2011). Down-regulation of *drp-1* in UAS-*hsc70-5* IR background [Fig. 4A(v,vi)] resulted in decrease in co-localizing mitochondria-lysosomal structures whereas co-expression of UAS-*pka* IR (cAMP-dependent PKA; pka-C1) in UAS-*hsc70-5* IR background increased lysotracker-marked acidic-compartment density [Fig. 4B(i)]. Treatment with 20-hydroxyecdysone in wing imaginal disc mimicking ecdysone pulse increased Lysotracker density leading to increased cell death (acridine orange-positive) in UAS-*hsc70-5* IR [Fig. S2A and B]. Similarly, abrupt increase in cell death of AMPs [Adult Midgut Progenitors (Micchelli et al., 2011), identified as UAS-mito-GFP positive cells driven with escargot-GAL4 (esg-GAL4)] was observed at 120hAED (after egg deposition) in both UAS-*opa1-like* IR and UAS-*hsc70-5* IR backgrounds [Fig. 4C and D] using the anti-cleaved caspase-3 antibody which specifically detects the cleaved active forms of the main effector caspases in *Drosophila* – Drice and Dcp-1 (Fan and Bergmann, 2010; Florentin and Arama, 2012; Yacobi-Sharon et al., 2013). AMPs appeared as small diploid cells in clusters (>8 Mito-GFP+ve cells) and were distinct from large polyploid midgut enterocytes (ECs) in Control. Interestingly, recombining hypomorphic allele of *dor* mutant [lysosomal biogenesis protein Deep-orange (*dor*^{4}); Fig. 4D; Yacobi-Sharon et al., 2013] in the UAS-*hsc70-5* IR background displayed a marked (15–25%) decrease in the number of AMPs positive with anti-cleaved caspase-3 antibody, suggesting a role for Lysosomes in AMPs death (also confirmed by acridine orange staining). Similar protection against AMPs death was observed when either *Opa1-FLAG* was over-expressed or *drp-1* was down-regulated in UAS-*hsc70-5* IR background [Fig. 4D].

Drosophila prepupal tissues like salivary gland, fat body, and larval-gut undergo precisely timed periods of programmed autophagy-mediated cell death (Rusten et al., 2004; Scott et al., 2007). Induction of pro-apoptotic molecules, like Hid and Reaper, by precisely timed ecdysone pulse induces autophagy leading to caspase activation; thereby triggering developmental programmed cell death (PCD; apoptosis) in *Drosophila* prepupal tissues (Yin and Thummel, 2005). Mitochondrial fragmentation has been a hallmark of upstream processes leading to apoptosis; defects in mitochondrial fragmentation or highly tubular state delays activation of caspases like Dronc, leading to reduction in developmental PCD in *drp-1* mutant's prepupal tissues (Goyal et al., 2007). Reduction in fusion capacity of depolarized mitochondria eventually targets it for degradation through autophagic pathway; however, inhibition of fission resulted in inhibition of mitochondrial autophagy or mitophagy. Fission at the advent of autophagy critically serves not only to produce small sized mitochondria, but also for mitochondrial turnover (Twig et al., 2008). Co-expression of UAS-*drp-1* IR with UAS-*hsc70-5* IR rescues mitochondrial morphology in the same way that over-expression of *Opa1-FLAG* in UAS-*hsc70-5* IR background does, but mitochondria of CSA < 0.3 μm^2 size continue to remain overlapped with Lysotracker with or without ecdysone treatment. This is in agreement with Twig et al. (2008) suggesting smaller fragments might still be fusion-incompetent due to proteolysed or degraded forms of OPA1 and are subjected to clearance. Mitochondria have been shown to regulate autophagy primarily through cAMP-dependent PKA since hyperactivation of PKA activity impairs induction of autophagy triggered by mitochondrial respiration defects (Graef and Nunnari, 2011). Down-regulation of *pka-C1* in UAS-*hsc70-5* IR background has increased lysosomal expression as compared to UAS-*drp-1* IR in UAS-*hsc70-5* IR background probably through regulation of PKA activity or levels of expression since membrane potential of UAS-*hsc70-5* IR is less compared to Control and mitochondrial fusion is minimal. The increase in lysosomal response on treatment of rapamycin in UAS-*pka* IR larval wing imaginal disc reveals a primary role for PKA in lysosomal-mediated autophagic regulation (Kalamidas et al., 2006) which, therefore, acts as a positive control for activation of autophagic pathway. Detecting autophagic process using LC3-tagged to a fluorescent molecule is an ideal tool and is used in cell lines (Twig et al., 2008); but, rather than distinct punctate structures, we observed dimming eGFP signal throughout the cell and some red fluorescence probably due to quenching of the eGFP in the acidic environment of the lysosomes in wing imaginal disc (data not shown, Nezis et al., 2010). It can be argued that the cell death reported in wing imaginal disc [Fig. S2] is via type II autophagic cell death because co-expression of UAS-*pka* IR and UAS-*hsc70-5* IR or TORC-inhibited by rapamycin increases Lysotracker density leading to cell death. cAMP-dependent PKA and TORC1 are regulators of autophagic induction and flux (Noda and Ohsumi, 1998; Budovskaya et al., 2004). On the other hand, either *Opa1-FLAG* over-expression or *drp-1* down-regulation in UAS-*hsc70-5* IR background results in protection against death [Figs. S2B and 4D].This suggests that mitochondrial dynamin family protein functions antagonistically to autophagy/lysosome-mediated cell death through regulation of mitochondrial morphology.

4. Conclusion

Using a targeted mitochondria-specific proteomic approach to screen for Opa1-like-interacting proteins we identified, for the first time in *Drosophila*, a novel interaction of Opa1-like with mtHsp70 cognate subunit 5/Mortalin along with other bonafide interactors (also known to interact with OPA1 in other model systems; Guillery et al., 2008; Darshi et al., 2011). Here, we demonstrate that Opa1-like influences mitochondrial morphology through its interaction with Marf and dMitofilin in an ATP-dependent manner. Mitochondrial dysfunction in *hsc70-5* depleted background leads to proteolysis of Opa1-like and thereby induces mitochondrial fragmentation and degradation. Thus, Hsc70-5 seems to function upstream of Opa1-like-mediated effects on mitochondrial morphogenesis. Over-expression of Opa1-like not only rescues mitochondrial morphology but also reverses the lysosomal-mediated cell death in *hsc70-5* knock-down background in both differentiated and precursor stem cells in *Drosophila*. The observations match our hypothesis that *Hsc70-5*, like mammalian Mortalin, acts in signaling pathways responsible for the maintenance of mitochondrial morphology and mitochondrial stress response. Regulation of mitochondrial morphology is, therefore, a crucial determinant of cellular homeostasis.

Acknowledgements

We are grateful to Dr. Richa Rikhy (IISER, Pune) and Prof. Madan Rao (NCBS, Bangalore) for critical comments on the manuscript. We thank Bloomington Stock Center (Indiana Univ.), Vienna Drosophila RNAi Center (Vienna) and NCBS Fly Stock Center for fly strains. We would like to acknowledge DBS-TIFR for reagents and antibodies. We thank Swagata Dey (DBS-TIFR, Mumbai) and Aparna Sherlekar (IISER, Pune) for helping us with imaging at DBS-TIFR and IISER, respectively. We thank Dr. Jongkyeong Chung (KIASK, Korea) for providing pUAS-Opa1-FLAG. Special thanks to Dr. Mahendra Sonawane and his lab members, Dr. Maithreyi Narasimha and Dr. Krishanu Ray for inputs during the study.

S.B. is grateful to Prof. Shobhona Sharma, Prof. Satyajit Mayor, Prof. Vijay Raghavan, and Prof. Apurva Sarin for their support. S.B. thanks Dr. Mahendra Sonawane for providing lab space and partial funding for the project at DBS-TIFR. S.B. thanks family and friends for their support. S.B. also thanks Balaji Chinthapalli for helping in mass-spectrometry. This work was supported by intramural grants of TIFR.

Appendix A. Supplementary data

Supplementary data associated with this article can be found, in the online version, at http://dx.doi.org/10.1016/j.biocel.2014.05.041.

References

Alonso J, Rodriguez JM, Baena-Lopez LA, Santarén JF. Characterization of the *Drosophila melanogaster* mitochondrial proteome. J Proteome Res 2005;4(5):1636–45.

Amutha B, Gordon DM, Gu Y, Pain D. A novel role of Mgm1p, a dynamin-related GTPase, in ATP synthase assembly and cristae formation/maintenance. Biochem J 2004;381(Pt1):19–23.

Baricault L, Ségui B, Guégand L, Olichon A, Valette A, Larminat F, et al. OPA1 cleavage depends on decreased mitochondrial ATP level and bivalent metals. Exp Cell Res 2007;313(17):3800–8.

Bereiter-Hahn J, Voth M. Dynamics of mitochondria in living cells: shape changes, dislocations, fusion, and fission of mitochondria. Microsc Res Tech 1994;27(3):198–219.

Benard G, Bellance N, James D, Parrone P, Fernandez H, Letellier T, Rossignol R. Mitochondrial bioenergetics and structural network organization. J Cell Sci 2007;120(Pt 5):838–48.

Budovskaya YV, Stephan JS, Reggiori F, Klionsky DJ, Herman PK. The Ras/cAMP-dependent protein kinase signaling pathway regulates an early step of the autophagy process in *Saccharomyces cerevisiae*. J Biol Chem 2004;279(20):20663–71.

Burbulla LF, Schelling C, Kato H, Rapaport D, Woitalla D, Schiesling C, et al. Dissecting the role of the mitochondrial chaperone mortalin in Parkinson's disease: functional impact of disease-related variants on mitochondrial homeostasis. Hum Mol Genet 2010;19(22):4437–52.

Chen TH, Kambal A, Krysiak K, Walshauser MA, Raju G, Tibbitts JF, et al. Knockdown of Hspa9, a del(5q31.2) gene, results in a decrease in hematopoietic progenitors in mice. Blood 2011;117(5):1530–9.

Choi SY, Huang P, Jenkins GM, Chan DC, Schiller J, Frohman MA. A common lipid links Mfn-mediated mitochondrial fusion and SNARE-regulated exocytosis. Nat Cell Biol 2006;8(11):1255–62.

Cipolat S, Martins BO, Dal ZB, Scorrano L. OPA1 requires mitofusin 1 to promote mitochondrial fusion. Proc Natl Acad Sci U S A 2004;101(45):15927–32.

Danial NN, Korsmeyer SJ. Cell death: critical control points. Cell 2004;116(2):205–19.

Darshi M, Mendiola VL, Mackey MR, Murphy AN, Koller A, Perkins GA, et al. ChChd3, an inner mitochondrial membrane protein, is essential for maintaining crista integrity and mitochondrial function. J Biol Chem 2011;286(4):2918–32.

Deng H, Dodson MW, Huang H, Guo M. The Parkinson's disease genes pink1 and parkin promote mitochondrial fission and/or inhibit fusion in Drosophila. Proc Natl Acad Sci U S A 2008;105(38):14503–8.

De Vos KJ, Allan VJ, Grierson AJ, Sheetz MP. Mitochondrial function and actin regulate dynamin-related protein 1-dependent mitochondrial fission. Curr Biol 2005;15(7):678–83.

Dietzl G, Chen D, Schnorrer F, Su KC, Barinova Y, Fellner M, et al. A genome-wide transgenic RNAi library for conditional gene inactivation in Drosophila. Nature 2007;448(7150):151–6.

Dorn GW II, Clark CF, Eschenbacher WH, Kang MY, Engelhard JT, Warner SJ, et al. MARF and Opa1 control mitochondrial and cardiac function in Drosophila. Circ Res 2011;108(1):12–7.

Duvezin-Caubet S, Jagasia R, Wagener J, Hofmann S, Trifunovic A, Hansson A, et al. Proteolytic processing of OPA1 links mitochondrial dysfunction to alterations in mitochondrial morphology. J Biol Chem 2006;281(49):37972–9.

Ehses S, Raschke I, Mancuso G, Bernacchia A, Geimer S, Tondera D, et al. Regulation of OPA1 processing and mitochondrial fusion by m-AAA protease isoenzymes and OMA1. J Cell Biol 2009;187(7):1023–36.

Elmore SP, Qian T, Grissom SF, Lemasters JJ. The mitochondrial permeability transition initiates autophagy in rat hepatocytes. FASEB J 2001;15(12):2286–7.

Fan Y, Bergmann A. The cleaved-Caspase-3 antibody is a marker of Caspase-9-like DRONC activity in Drosophila. Cell Death Differ 2010;17(3):534–9.

Florentin A, Arama E. Caspase levels and execution efficiencies determine the apoptotic potential of the cell. J Cell Biol 2012;196(4):513–27.

Frezza C, Cipolat S, Martins BO, Micaroni M, Beznoussenko GV, Rudka T, et al. OPA1 controls apoptotic cristae remodeling independently from mitochondrial fusion. Cell 2006;126(1):177–89.

Gomes LC, Di BG, Scorrano L. During autophagy mitochondria elongate, are spared from degradation and sustain cell viability. Nat Cell Biol 2011;13(5):589–98.

Goyal G, Fell B, Sarin A, Youle RJ, Sriram V. Role of mitochondrial remodeling in programmed cell death in *Drosophila melanogaster*. Dev Cell 2007;12(5):807–16.

Graef M, Nunnari J. Mitochondria regulate autophagy by conserved signalling pathways. EMBO J 2011;30(11):2101–14.

Guillery O, Malka F, Landes T, Guillou E, Blackstone C, Lombès A, et al. Metalloprotease-mediated OPA1 processing is modulated by the mitochondrial membrane potential. Biol Cell 2008;100(5):315–25.

Imoto M, Tachibana I, Urrutia R. Identification and functional characterization of a novel human protein highly related to the yeast dynamin-like GTPase Vps1J. Cell Sci 1998;111(Pt 10):1341–9.

Ishihara N, Fujita Y, Oka T, Mihara K. Regulation of mitochondrial morphology through proteolytic cleavage of OPA1. EMBO J 2006;25(13):2966–77.

Iyengar B, Luo N, Farr CL, Kaguni LS, Campos AR. The accessory subunit of DNA polymerase gamma is essential for mitochondrial DNA maintenance and development in *Drosophila melanogaster*. Proc Natl Acad Sci U S A 2002;99(7):4483–8.

Jahani-Asl A, Pilon-Larose K, Xu W, MacLaurin JG, Park DS, McBride HM, et al. The mitochondrial inner membrane GTPase, optic atrophy 1 (Opa1), restores mitochondrial morphology and promotes neuronal survival following excitotoxicity. J Biol Chem 2011;286(6):4772–82.

Kalamidas SA, Kuehnel MP, Peyron P, Rybin V, Rauch S, Kotoulas OB, et al. cAMP synthesis and degradation by phagosomes regulate actin assembly and fusion events: consequences for mycobacteria. J Cell Sci 2006;119(Pt 17):3686–94.

Kawai A, Nishikawa S, Hirata A, Endo T. Loss of the mitochondrial Hsp70 functions causes aggregation of mitochondria in yeast cells. J Cell Sci 2001;114(Pt 19):3565–74.

Karbowski M, Lee YJ, Gaume B, Jeong SY, Frank S, Nechushtan A, et al. Spatial and temporal association of Bax with mitochondrial fission sites, Drp1, and Mfn2 during apoptosis. J Cell Biol 2002;159(6):931–8.

Kaul SC, Deocaris CC, Wadhwa R. Three faces of mortalin: a housekeeper, guardian and killer. Exp Gerontol 2007;42(4):263–74.

Kieper N, Holmström KM, Ciceri D, Fiesel FC, Wolburg H, Ziviani E, et al. Modulation of mitochondrial function and morphology by interaction of Omi/HtrA2 with the mitochondrial fusion factor OPA1. Exp Cell Res 2010;316(7):1213–24.

Legros F, Lombès A, Frachon P, Rojo M. Mitochondrial fusion in human cells is efficient, requires the inner membrane potential, and is mediated by mitofusins. Mol Biol Cell 2002;13(12):4343–54.

Liu Y, Liu W, Song XD, Zuo J. Effect of GRP75/mthsp70/PBP74/mortalin overexpression on intracellular ATP level, mitochondrial membrane potential and ROS accumulation following glucose deprivation in PC12 cells. Mol Cell Biochem 2005;268(1–2):45–51.

McQuibban GA, Lee JR, Zheng L, Juusola M, Freeman M. Normal mitochondrial dynamics requires rhomboid-7 and affects Drosophila lifespan and neuronal function. Curr Biol 2006;16(10):982–9.

Meeusen S, McCaffery JM, Nunnari J. Mitochondrial fusion intermediates revealed in vitro. Science 2004;305(5691):1747–52.

Meisinger C, Sommer T, Pfanner N. Purification of *Saccharomcyes cerevisiae* mitochondria devoid of microsomal and cytosolic contaminations. Anal Biochem 2000;287(2):339–42.

Micchelli CA, Sudmeier L, Perrimon N, Tang S, Beehler-Evans R. Identification of adult midgut precursors in Drosophila. Gene Expr Patterns 2011;11(1–2):12–21.

Neupert W, Brunner M. The protein import motor of mitochondria. Nat Rev Mol Cell Biol 2002;3(8):555–65.

Nezis IP, Shravage BV, Sagona AP, Lamark T, Bjørkøy G, Johansen T, et al. Autophagic degradation of dBruce controls DNA fragmentation in nurse cells during late *Drosophila melanogaster* oogenesis. J Cell Biol 2010;190(4):523–31.

Noda T, Ohsumi Y. Tor, a phosphatidylinositol kinase homologue, controls autophagy in yeast. J Biol Chem 1998;273(7):3963–6.

Noguchi T, Koizumi M, Hayashi S. Sustained elongation of sperm tail promoted by local remodeling of giant mitochondria in Drosophila. Curr Biol 2011;21(10):805–14.

Nunnari J, Marshall WF, Straight A, Murray A, Sedat JW, Walter P. Mitochondrial transmission during mating in *Saccharomyces cerevisiae* is determined by mitochondrial fusion and fission and the intramitochondrial segregation of mitochondrial DNA. Mol Biol Cell 1997;8(7):1233–42.

Olichon A, Emorine LJ, Descoins E, Pelloquin L, Brichese L, Gas N, et al. The human dynamin-related protein OPA1 is anchored to the mitochondrial inner membrane facing the inter-membrane space. FEBS Lett 2002;523(1–3):171–6.

O'Reilly CM, Fogarty KE, Drummond RM, Tuft RA, Walsh JV. Quantitative analysis of spontaneous mitochondrial depolarizations. Biophys J 2003;85(5):3350–7.

Park J, Lee G, Chung J. The PINK1-Parkin pathway is involved in the regulation of mitochondrial remodeling process. Biochem Biophys Res Commun 2009;378(3):518–23.

Pilling AD, Horiuchi D, Lively CM, Saxton WM. Kinesin-1 and Dynein are the primary motors for fast transport of mitochondria in Drosophila motor axons. Mol Biol Cell 2006;17(4):2057–68.

Rabl R, Soubannier V, Scholz R, Vogel F, Mendl N, Vasiljev-Neumeyer A, et al. Formation of cristae and crista junctions in mitochondria depends on antagonism between Fcj1 and Su e/g. J Cell Biol 2009;185(6):1047–63.

Rahman M, Kylsten P. Rhomboid-7 over-expression results in Opa1-like processing and malfunctioning mitochondria. Biochem Biophys Res Commun 2011;414(2):315–20.

Rana A, Rera M, Walker DW. Parkin overexpression during aging reduces proteotoxicity, alters mitochondrial dynamics, and extends lifespan. Proc Natl Acad Sci U S A 2013;110(21):8638–43.

Rizzuto R, Bernardi P, Pozzan T. Mitochondria as all-round players of the calcium game. J Physiol 2000;529(Pt 1):37–47.

Rusten TE, Lindmo K, Juhász G, Sass M, Seglen PO, Brech A, et al. Programmed autophagy in the Drosophila fat body is induced by ecdysone through regulation of the PI3K pathway. Dev Cell 2004;7(2):179–92.

Santel A, Fuller MT. Control of mitochondrial morphology by a human mitofusin. J Cell Sci 2001;114(Pt 5):867–74.

Schwarzer C, Barnikol-Watanabe S, Thinnes FP, Hilschmann N. Voltage-dependent anion-selective channel (VDAC) interacts with the dynein light chain Tctex1 and the heat-shock protein PBP74. Int J Biochem Cell Biol 2002;34(9):1059–70.

Scott RC, Schuldiner O, Neufeld TP. Role and regulation of starvation-induced autophagy in the Drosophila fat body. Dev Cell 2004;7(2):167–78.

Scott RC, Juhász G, Neufeld TP. Direct induction of autophagy by Atg1 inhibits cell growth and induces apoptotic cell death. Curr Biol 2007;17(1):1–11.
Sesaki H, Southard SM, Yaffe MP, Jensen RE. Mgm1p, a dynamin-related GTPase, is essential for fusion of the mitochondrial outer membrane. Mol Biol Cell 2003;14(6):2342–56.
Söding J, Biegert A, Lupas AN. The HHpred interactive server for protein homology detection and structure prediction. Nucleic Acids Res 2005;33(Web Server issue):W244–8.
Song Z, Chen H, Fiket M, Alexander C, Chan DC. OPA1 processing controls mitochondrial fusion and is regulated by mRNA splicing, membrane potential, and Yme1L. J Cell Biol 2007;178(5):749–55.
Szabadkai G, Bianchi K, Varnai P, De Stefani D, Wieckowski MR, Cavagna D, et al. Chaperone-mediated coupling of endoplasmic reticulum and mitochondrial Ca^{2+} channels. J Cell Biol 2006;175(6):901–11.
Tang S, Le PK, Tse S, Wallace DC, Huang T. Heterozygous mutation of Opa1 in Drosophila shortens lifespan mediated through increased reactive oxygen species production. PLoS One 2009;4(2):e4492.
Tatsuta T, Langer T. Quality control of mitochondria: protection against neurodegeneration and ageing. EMBO J 2008;27(2):306–14.
Twig G, Elorza A, Molina AJ, Mohamed H, Wikstrom JD, Walzer G, et al. Fission and selective fusion govern mitochondrial segregation and elimination by autophagy. EMBO J 2008;27(2):433–46.
von der Malsburg K, Müller JM, Bohnert M, Oeljeklaus S, Kwiatkowska P, Becker T, et al. Dual role of mitofilin in mitochondrial membrane organization and protein biogenesis. Dev Cell 2011;21(4):694–707.
Wong ED, Wagner JA, Scott SV, Okreglak V, Holewinske TJ, Cassidy-Stone A, et al. The intramitochondrial dynamin-related GTPase, Mgm1p, is a component of a protein complex that mediates mitochondrial fusion. J Cell Biol 2003;160(3):303–11.
Yacobi-Sharon K, Namdar Y, Arama E. Alternative germ cell death pathway in Drosophila involves HtrA2/Omi, lysosomes, and a caspase-9 counterpart. Dev Cell 2013;25(1):29–42.
Yang RF, Zhao GW, Liang ST, Zhang Y, Sun LH, Chen HZ, Liu DP. Mitofilin regulates cytochrome c release during apoptosis by controlling mitochondrial cristae remodeling. Biochem Biophys Res Commun 2012;428(1):93–8.
Yin VP, Thummel CS. Mechanisms of steroid-triggered programmed cell death in Drosophila. Semin Cell Dev Biol 2005;16(2):237–43.
Zhu JY, Vereshchagina N, Sreekumar V, Burbulla LF, Costa AC, Daub KJ, et al. Knockdown of Hsc70-5/mortalin induces loss of synaptic mitochondria in a Drosophila Parkinson's disease model. PLoS One 2013;8(12):e83714.
Ziviani E, Tao RN, Whitworth AJ. Drosophila parkin requires PINK1 for mitochondrial translocation and ubiquitinates mitofusin. Proc Natl Acad Sci U S A 2010;107(11):5018–23.